AAS 09-391

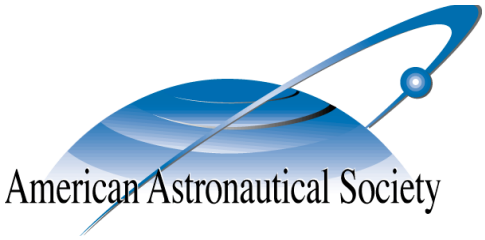

American Institute of
Aeronautics and Astronautics

SWITCHED LYAPUNOV FUNCTION BASED COULOMB CONTROL OF A TRIANGULAR 3-VEHICLE CLUSTER

Shuquan Wang and Hanspeter Schaub

AAS/AIAA Astrodynamics Specialist Conference

Pittsburgh, Pennsylvania August 9–13, 2009

AAS Publications Office, P.O. Box 28130, San Diego, CA 92198

(Preprint) AAS 09-391

SWITCHED LYAPUNOV FUNCTION BASED COULOMB CONTROL OF A TRIANGULAR 3-VEHICLE CLUSTER

Shuquan Wang* **and Hanspeter Schaub†**

This paper studies a three-body Coulomb virtual structure control problem. For a formation of three spacecraft flying freely in deep space, actively controlled Coulomb forces are used to stabilize the formation shape to a desired triangular configuration. The control problem is challenging because the system is nonlinear and nonaffine, while the direct control of all three sides at the same time is often not implementable using only real charges. Firstly, a two-side switched control strategy is developed to control the two sides with the worst shape errors such that the implementable charge control solution is guaranteed. However, analytical and practical stability issues arise due to the discrete control time steps. Using the multiple Lyapunov functions analysis tool, a stable switched control strategy is setup in a manner such that the activated error function is decreasing rapidly enough to compensate for a potentially increased amount during the last uncontrolled control cycle. Thus all the error functions are made *Lyapunov-like* and the global stability of the switched control strategy is guaranteed. Perfect convergence to desired triangular shape is not physically achievable with Coulomb forces alone because the triangle is not a natural equilibrium solution. Numerical simulations illustrate the effectiveness of the stable switched control strategy.

INTRODUCTION

A spacecraft virtual structure is a cluster or formation of spacecraft with a fixed relative configuration forming a desired shape to satisfy mission sensor requirements. A feedback control strategy is required to stabilize the spacecraft to the reference configuration. The goal is to be able to place sensors at desired locations to provide the required baselines to satisfy mission objectives. The free-flying concept is attractive in that it allows for large sensor baselines to be considered, and the overall cluster shape can be changed over time to accommodate changing mission sensing requirements. The virtual structure approach is a convenient method to prescribe a coordinated behavior of the formation. Reference 1 develops a formation feedback control strategy to achieve the virtual structure control. The authors at first assume that a rigid structure is in orbit, then use an inverse dynamics method to determine a feedforward reference control using thrusters that can maintain the spacecraft in the rigid structure configuration. At last a feedback control loop is utilized to stabilize the spacecraft cluster about the virtual structure. This virtual structure control is based on the thrusters' capability to control the three-dimensional motions of the satellites.

In contrast, this paper studies a Coulomb virtual structure control problem. As compared to the traditional virtual structure control, Coulomb virtual structure control is a very different problem because the direct controllability of the relative satellite positions is not present. A Coulomb virtual structure uses only electrostatic forces (Coulomb forces) to control the shape of the formation, and not necessarily the formation's inertial position and orientation. The use of Coulomb forces to control spacecraft relative motion was first investigated by King et. al. in 2002.[2] Since then a lot of applications of the Coulomb formation flying (CFF) concept have been studied. These include CFF equilibrium solutions,[3,4,5,6] 2-craft Coulomb tether control,[7,8,9,10] hybrid propulsion strategy combining Coulomb forces and elestric thrusters,[11] as well as spacecraft collision avoidance using Coulomb forces.[12,13,14]

The studies of open-loop equilibrium charge solutions and Coulomb virtual tether control are related to Coulomb virtual structure control, but they focus on different aspects. The Coulomb tether papers present the

*Graduate Research Assistant, Aerospace Engineering Sciences Department, University of Colorado, Boulder, CO.
†Associate Professor, H. Joseph Smead Fellow, Aerospace Engineering Sciences Department, University of Colorado, Boulder, CO.

first examples of feedback stabilized virtual Coulomb structures.[7,8,9,10] However, their control methodology does not scale to systems with more than 2 spacecraft. References 15, 16 and 17 are more closely related to the Coulomb virtual structure control problem considered in this paper. Reference 15 studies constant charge invariant shape solutions for spinning three craft Coulomb formation. It shows that only the collinear configuration and expanding equilateral triangle configuration can be invariant assuming a fixed spacecraft potential. Reference 16 introduces the spinning 2-craft Coulomb tether concept. It is the first work that analyses the open-loop stability of a Coulomb tether with constant spacecraft charges, based on a linearized model. Assuming the Coulomb tether flying in deep space, it shows that the radial motion is locally stable if the spacecraft separation distance is less then the Debye length. Reference 17 studies the three-craft Coulomb tether problem. Based on a linearized model about a collinear equilibrium configuration, a linear feedback control is developed to stabilize the Coulomb tether to the collinear relative equilibria. The nonlinear system converges to a neighborhood of the desired equilibrium, but due to the approximation using linearization technique, the size of the convergence neighborhood is limited. General triangular formation shapes, or non-equiblibrium collinear shapes, are not feasible with this control strategy.

Reference 18 studies a one-dimensionally constrained three-craft Coulomb virtual structure control. Here a two stage control strategy is developed to make the 1D three-craft formation converge to a desired configuration. The first stage uses saturated control to stabilize the relative motion of the formation. After the relative motion is stabilized, the second stage is engaged to control the shape of the formation to converge to the desired shape. The control convergence domains are found numerically. But for a symmetric configuration case, analytical criterion is derived analytically. The 1D nature of this work allows for significant mathematical simplifications, and provides for a dynamical system where solving for the charge products always leads to real and unique individual charge solutions.

This paper extends the work in Reference 18 into three-dimensional space. This results in a significant increase in the complexity of the dynamical system, as well as the control implementation. While the products of the spacecraft charges appear linearly in the dynamics, the mapping to individual charges can yield at times imaginary solutions. Thus a standard inverse dynamics solution is not feasible here. Instead, a Lyapunov-based nonlinear control strategy is sought which stabilizes the configuration of the 3-craft formation to an arbitrary triangular shape. Because the individual spacecraft charges appear in a nonlinear and coupled form in the equations of motion, a simple control strategy that controls three side lengths at once may result in imaginary charges, which is not implementable. This paper investigates how to develop an implementable control strategy while still ensuring the stability of the system. One method to guarantee an implementable control is to always control the worst two triangle sides. However, such switching strategy can cause stability issues due to the discrete control time steps. Multiple Lyapunov functions analysis is a tool to analyze the stability of a switched system. This paper investigates how to modify the switched control strategy such that the stability of the charged spacecraft virtual structure system is ensured. Numerical simulations illustrate the closed-loop performance of the new 3-craft charge control strategy.

SEPARATION DISTANCE EQUATIONS OF MOTION

This paper considers three spacecraft flying in 3-dimensional free space where there are no external forces acting on the system. The scenario of the 3-body Coulomb virtual structure is shown in Figure 1. Assuming point-charge models for the spacecraft, the Coulomb force between the i^{th} and j^{th} spacecraft exerted by the i^{th} spacecraft is given by:[14]

$$\boldsymbol{F}_{ij} = -k_c \frac{q_i q_j}{r_{ij}^2} \left(1 + \frac{r_{ij}}{\lambda_{\text{d}}}\right) e^{-\frac{r_{ij}}{\lambda_{\text{d}}}} \hat{\boldsymbol{e}}_{ij} \tag{1}$$

where $k_c = 8.99 \times 10^9 \ \text{Nm}^2\text{C}^{-2}$ is the Coulomb constant, q_i is the charge of the i^{th} spacecraft which can be actively controlled, $r_{ij} = \|\boldsymbol{r}_{ij}\|$ is the separation distance between the i^{th} and j^{th} spacecraft. The parameter λ_{d} is the Debye length which characterizes the plasma shielding effect, while $\hat{\boldsymbol{e}}_{ij}$ is the unit vector pointing from the i^{th} to j^{th} spacecraft. In developing the control algorithm, it's assumed that $\lambda_{\text{d}} = \infty$ which indicates that the plasma shielding effect is not explicitly considered. As a result, the separation distance must be less than the local Debye length. At 1 AU the Debye length can range from 30-50 meters.

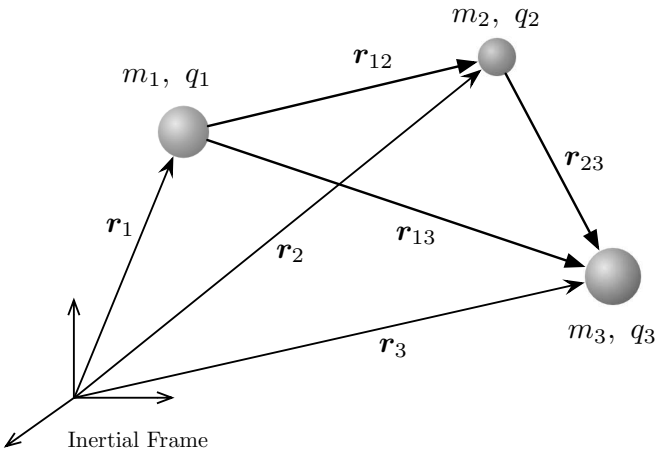

Figure 1. Scenario of the 3-body system.

By the assumption that there are no external forces acting on the 3-body system, the inertial equations of motion (EOMs) are given by:

$$m_1\ddot{\boldsymbol{r}}_1 = -k_c\frac{q_1q_2}{r_{12}^2}\hat{\boldsymbol{e}}_{12} - k_c\frac{q_1q_3}{r_{13}^2}\hat{\boldsymbol{e}}_{13} \tag{2a}$$

$$m_2\ddot{\boldsymbol{r}}_2 = k_c\frac{q_1q_2}{r_{12}^2}\hat{\boldsymbol{e}}_{12} - k_c\frac{q_2q_3}{r_{23}^2}\hat{\boldsymbol{e}}_{23} \tag{2b}$$

$$m_3\ddot{\boldsymbol{r}}_3 = k_c\frac{q_1q_3}{r_{13}^2}\hat{\boldsymbol{e}}_{13} + k_c\frac{q_2q_3}{r_{23}^2}\hat{\boldsymbol{e}}_{23} \tag{2c}$$

where m_i is the mass of the i^{th} spacecraft, $\boldsymbol{r}_i$ is the inertial position of the i^{th} spacecraft.

This paper intends to develop a control algorithm to make the 3-body formation assume a certain desired shape. The shape of a 3-body formation can be completely defined by the three separation distances between any two spacecraft. This paper defines the goal of the control to be making the three separation distances $(r_{12}, r_{23}, r_{13})^T$ converge to the desired distances $(r_{12}^*, r_{23}^*, r_{13}^*)^T$. The first step is to identify the separation distances' EOMs.

For the convenience of notation, a vector $\boldsymbol{\xi}$ is defined as a function of the charge products:

$$\boldsymbol{\xi} = (\xi_1,\ \xi_2,\ \xi_3)^T = \left(k_c\frac{q_1q_2}{r_{12}^2},\ k_c\frac{q_2q_3}{r_{23}^2},\ k_c\frac{q_1q_3}{r_{13}^2}\right)^T \tag{3}$$

Based on the inertial EOM in Eq. (2), the relative positions' EOMs are found:

$$\ddot{\boldsymbol{r}}_{12} = \ddot{\boldsymbol{r}}_2 - \ddot{\boldsymbol{r}}_1 = \xi_1\left(\frac{1}{m_1}+\frac{1}{m_2}\right)\hat{\boldsymbol{e}}_{12} - \xi_2\frac{1}{m_2}\hat{\boldsymbol{e}}_{23} + \xi_3\frac{1}{m_1}\hat{\boldsymbol{e}}_{13} \tag{4a}$$

$$\ddot{\boldsymbol{r}}_{23} = \ddot{\boldsymbol{r}}_3 - \ddot{\boldsymbol{r}}_2 = -\xi_1\frac{1}{m_2}\hat{\boldsymbol{e}}_{12} + \xi_2\left(\frac{1}{m_2}+\frac{1}{m_3}\right)\hat{\boldsymbol{e}}_{23} + \xi_3\frac{1}{m_3}\hat{\boldsymbol{e}}_{13} \tag{4b}$$

$$\ddot{\boldsymbol{r}}_{13} = \ddot{\boldsymbol{r}}_3 - \ddot{\boldsymbol{r}}_1 = \xi_1\frac{1}{m_1}\hat{\boldsymbol{e}}_{12} + \xi_2\frac{1}{m_3}\hat{\boldsymbol{e}}_{23} + \xi_3\left(\frac{1}{m_1}+\frac{1}{m_3}\right)\hat{\boldsymbol{e}}_{13} \tag{4c}$$

The relationship between the separation distance's acceleration $\ddot{r}_{ij}$ and the relative acceleration $\ddot{\boldsymbol{r}}_{ij}$ is achieved by differentiating the identity $r_{ij} = \sqrt{\boldsymbol{r}_{ij}\cdot\boldsymbol{r}_{ij}}$ twice:

$$\ddot{r}_{ij} = \ddot{\boldsymbol{r}}_{ij}\cdot\hat{\boldsymbol{e}}_{ij} + \frac{1}{r_{ij}}\|\dot{\boldsymbol{r}}_{ij}\|^2\Big(1-\cos^2\angle(\boldsymbol{r}_{ij},\ \dot{\boldsymbol{r}}_{ij})\Big) \tag{5}$$

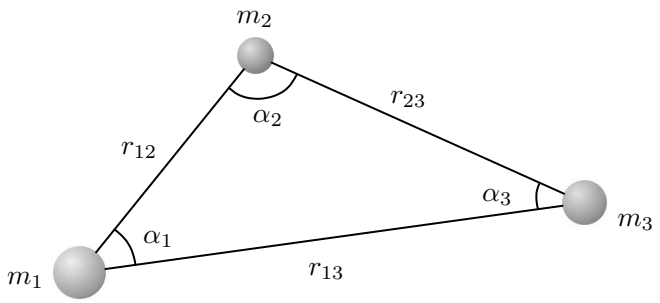

Figure 2. Geometry of the 3-body system.

Substituting the relative positions' EOMs in Eq. (4) into Eq. (5), yields the separation distances' EOMs:

$$\ddot{r}_{12} = \xi_1 \left(\frac{1}{m_1} + \frac{1}{m_2} \right) + \xi_2 \frac{1}{m_2} \cos\alpha_2 + \xi_3 \frac{1}{m_1} \cos\alpha_1 + f_1 \tag{6a}$$

$$\ddot{r}_{23} = \xi_1 \frac{1}{m_2} \cos\alpha_2 + \xi_2 \left(\frac{1}{m_2} + \frac{1}{m_3} \right) + \xi_3 \frac{1}{m_3} \cos\alpha_3 + f_2 \tag{6b}$$

$$\ddot{r}_{13} = \xi_1 \frac{1}{m_1} \cos\alpha_1 + \xi_2 \frac{1}{m_3} \cos\alpha_3 + \xi_3 \left(\frac{1}{m_1} + \frac{1}{m_3} \right) + f_3 \tag{6c}$$

where α_i is the angle of the two sides cornered at the i^{th} spacecraft as shown in Figure 2, f_i is the shortcut:

$$f_1 = \|\dot{\boldsymbol{r}}_{12}\|^2 \Big(1 - \cos^2 \angle(\boldsymbol{r}_{12},\ \dot{\boldsymbol{r}}_{12}) \Big) \tag{7a}$$

$$f_2 = \|\dot{\boldsymbol{r}}_{23}\|^2 \Big(1 - \cos^2 \angle(\boldsymbol{r}_{23},\ \dot{\boldsymbol{r}}_{23}) \Big) \tag{7b}$$

$$f_3 = \|\dot{\boldsymbol{r}}_{13}\|^2 \Big(1 - \cos^2 \angle(\boldsymbol{r}_{13},\ \dot{\boldsymbol{r}}_{13}) \Big) \tag{7c}$$

VIRTUAL STRUCTURE CONTROL STRATEGY

The goal of the virtual structure control is to make the separation distances converge to the given desired distances:

$$(r_{12},\ r_{23},\ r_{13})^T \to (r_{12}^*,\ r_{23}^*,\ r_{13}^*)^T \tag{8}$$

This paper assumes that the desired shape of the 3-body system is stationary, which indicates r_{ij}^* are constant. Using the state vector $\boldsymbol{X} = (r_{12},\ r_{23},\ r_{13})^T$, the separation distances' EOMs in Eq. (6) are rewritten into a concise form as:

$$\ddot{\boldsymbol{X}} = [B]\boldsymbol{\xi} + \boldsymbol{f} \tag{9}$$

where $\boldsymbol{f} = (f_1,\ f_2,\ f_3)^T$, and the matrix $[B]$ is

$$[B] = \begin{bmatrix} \left(\frac{1}{m_1} + \frac{1}{m_2}\right) & \frac{\cos\alpha_2}{m_2} & \frac{\cos\alpha_1}{m_1} \\ \frac{\cos\alpha_2}{m_2} & \left(\frac{1}{m_2} + \frac{1}{m_3}\right) & \frac{\cos\alpha_3}{m_3} \\ \frac{\cos\alpha_1}{m_1} & \frac{\cos\alpha_3}{m_3} & \left(\frac{1}{m_1} + \frac{1}{m_3}\right) \end{bmatrix} \tag{10}$$

Note that $[B]$ is diagonally dominant, so it's always invertible.

Define the state tracking error to be

$$\Delta\boldsymbol{X} = \boldsymbol{X} - \boldsymbol{X}^* \tag{11}$$

where $\boldsymbol{X}^* = (r_{12}^*,\ r_{23}^*,\ r_{13}^*)^T$ is the set of desired states.

The objective of the control is to find an implementable solution of $\boldsymbol{\xi}$ to make $\Delta\boldsymbol{X} \rightarrow \boldsymbol{0}$. Note that $\boldsymbol{\xi}$ is a linear function of the charge products. But the individual charges of spacecraft are the ultimate control inputs of the control system, which makes this a non-affine control problem. Not all the combinations of the charge products result in real solutions of individual charges, some combinations result in complex values of individual charges. Those complex solutions of individual charges are not physically implementable. This issue will be discussed and addressed later on.

3-Side Control Law

First, let us consider the case where all three sides are to be controlled at once. As will be seen, this control solution does not always exist due to the limited actuation capabilities of the Coulomb forces. Let us define a Lyapunov function candidate as

$$V = \frac{1}{2}\Delta\boldsymbol{X}^T[K]\Delta\boldsymbol{X} + \frac{1}{2}\Delta\dot{\boldsymbol{X}}^T\Delta\dot{\boldsymbol{X}} \tag{12}$$

where $[K]$ is a 3×3 positive definite matrix. Let us use $[K] = k[I_{3\times3}]$ for simplicity with $k > 0$ being constant. Taking a first-order time derivative of V and utilizing the EOMs in Eq. (9), yields:

$$\begin{aligned}\dot{V} &= \Delta\dot{\boldsymbol{X}}^T\big([K]\Delta\boldsymbol{X} + \Delta\ddot{\boldsymbol{X}}\big) \\ &= \Delta\dot{\boldsymbol{X}}^T\big([K]\Delta\boldsymbol{X} + [B]\boldsymbol{\xi} + \boldsymbol{f}\big)\end{aligned} \tag{13}$$

To guarantee overall stability set $\dot{V}$ to be a negative semi-definite function:

$$\dot{V} = -\Delta\dot{\boldsymbol{X}}^T[P]\Delta\dot{\boldsymbol{X}} \tag{14}$$

where $[P]$ is a 3×3 positive definite matrix. Note that this form of $\dot{V}$ is negative semi-definite, not negative definite because $V(\Delta\boldsymbol{X}, \Delta\dot{\boldsymbol{X}})$, but $\dot{V}$ is only explicitly a function of only $\Delta\dot{\boldsymbol{X}}$.

Substituting Eq. (14) into Eq. (13) and solving for $\boldsymbol{\xi}$, yields:

$$\boldsymbol{\xi} = [B]^{-1}(-[K]\Delta\boldsymbol{X} - \boldsymbol{f} - [P]\Delta\dot{\boldsymbol{X}}) \tag{15}$$

Note that even though $\dot{V}$ is negative semi-definite, the control law given by Eq. (15) is driving the state tracking error $\Delta\boldsymbol{X}$ converge to zero. This can be proved by the following two steps. Taking a second-order time derivative of V:

$$\ddot{V} = -2\Delta\dot{\boldsymbol{X}}^T[P]\Delta\ddot{\boldsymbol{X}} \tag{16}$$

When $\dot{V} = 0$ which indicates $\Delta\dot{\boldsymbol{X}}$, $\ddot{V} = 0$. Taking a third-order time derivative of V:

$$\dddot{V} = -2\Delta\ddot{\boldsymbol{X}}^T[P]\Delta\ddot{\boldsymbol{X}} - 2\Delta\dot{\boldsymbol{X}}^T[P]\Delta\dddot{\boldsymbol{X}} \tag{17}$$

When $\dot{V} = 0$, $\dddot{V} \leq 0$ and $\dddot{V} = 0$ only when $\Delta\boldsymbol{X} = \boldsymbol{0}$. Thus the system is asymptotically stable if the control law given by Eq. (15) can be implemented.

From the definition of $\boldsymbol{\xi}$ in Eq. (3), the individual charges are solved through:

$$\begin{cases} q_1 = & \sqrt{\frac{\xi_1\xi_3}{\xi_2 k_c}}\frac{|r_{12}r_{13}|}{|r_{23}|} \\ q_2 = & \text{sign}(\xi_2\xi_3)\sqrt{\frac{\xi_1\xi_2}{\xi_3 k_c}}\frac{|r_{12}r_{23}|}{|r_{13}|} \\ q_3 = & \text{sign}(\xi_3)\sqrt{\frac{\xi_2\xi_3}{\xi_1 k_c}}\frac{|r_{23}r_{13}|}{|r_{12}|} \end{cases} \tag{18}$$

Notice that Eq. (18) doesn't necessarily result in real solutions of the individual charges. If $\xi_1 \cdot \xi_2 \cdot \xi_3 < 0$, the individual charges are imaginary and are not physically implementable. By the definition in Eq. (3), $\xi_1 \cdot \xi_2 \cdot \xi_3 \propto (q_1 q_2 q_3)^2$. For an implementable solution of $\boldsymbol{\xi}$, the following inequality must be satisfied:

$$\xi_1 \cdot \xi_2 \cdot \xi_3 \geq 0 \tag{19}$$

However, the inequality in Eq. (19) is not guaranteed from the 3-side control algorithm in Eq. (15). Some special strategy has to be engaged to make the control algorithm physically implementable.

2-Side Control Switch Strategy

The previous section develops a Lyapunov-based control law that controls the three triangle side-lengths at once. The control is asymptotically stable, but it's not always physically implementable because at times it requires imaginary charges. If we control two sides at once instead of controlling three sides, correspondingly a subset of the state-space EOMs in Eq. (9) are considered, then the control input matrix $[B]$ becomes a 2×3 matrix. Utilizing the null space of the control input matrix, there is a family of solutions that have the same response. An implementable solution can always be found out from this solution family. The use of the null space of the input matrix to determine implementable real charge solutions is discussed in Reference 18.

This paper proposes a strategy that always controls the "worst" two sides of the triangle. By continuously switching to control the "worst" two sides, it's expected that the system is stabilized and the state tracking error converge to zero. However, the actual switching strategy must be carefully chosen to avoid making the system unstable. This paper defines the switching criterion by investigating the three sub-Lyapunov functions:

$$V_a = \frac{1}{2}k(\Delta X_1^2 + \Delta X_3^2) + \frac{1}{2}(\Delta X_1^2 + \Delta X_3^2) \triangleq \frac{k}{2}\Delta \boldsymbol{X}_a^T \Delta \boldsymbol{X}_a + \frac{1}{2}\Delta \dot{\boldsymbol{X}}_a^T \Delta \dot{\boldsymbol{X}}_a \tag{20a}$$

$$V_b = \frac{1}{2}k(\Delta X_1^2 + \Delta X_2^2) + \frac{1}{2}(\Delta X_1^2 + \Delta X_2^2) \triangleq \frac{k}{2}\Delta \boldsymbol{X}_b^T \Delta \boldsymbol{X}_b + \frac{1}{2}\Delta \dot{\boldsymbol{X}}_b^T \Delta \dot{\boldsymbol{X}}_b \tag{20b}$$

$$V_c = \frac{1}{2}k(\Delta X_2^2 + \Delta X_3^2) + \frac{1}{2}(\Delta X_2^2 + \Delta X_3^2) \triangleq \frac{k}{2}\Delta \boldsymbol{X}_c^T \Delta \boldsymbol{X}_c + \frac{1}{2}\Delta \dot{\boldsymbol{X}}_c^T \Delta \dot{\boldsymbol{X}}_c \tag{20c}$$

The subscripts $(a,\ b,\ c)$ denote the errors of the two sides cornered at the (1st, 2nd, 3rd) spacecraft respectively. The final Lyapunov function candidate being activated is chosen to be the largest sub-Lyapunov function:

$$V_{\text{ctrl}} = \max\{V_a,\ V_b,\ V_c\} \tag{21}$$

Once the control $\boldsymbol{\xi}$ is determined, the motions of the three sides are determined by Eq. (9). In order to develop a control algorithm to only stabilize two sides at once, the dynamics of the two sides being controlled are:

$$\ddot{\boldsymbol{X}}_{\text{ctrl}} = [B_{\text{ctrl}}]\boldsymbol{\xi} + \boldsymbol{f}_{\text{ctrl}} \tag{22}$$

where $[B_{\text{ctrl}}]$ is a 2×3 matrix with the two rows selected from the matrix $[B]$ according to the two sides being controlled.

Taking a first-order time derivative of V_{ctrl}, yields:

$$\dot{V}_{\text{ctrl}} = \Delta \dot{\boldsymbol{X}}_{\text{ctrl}}^T \big(k\Delta \boldsymbol{X}_{\text{ctrl}} + [B_{\text{ctrl}}]\boldsymbol{\xi} + \boldsymbol{f}_{\text{ctrl}}\big) \tag{23}$$

We force $\dot{V}_{\text{ctrl}}$ to be

$$\dot{V}_{\text{ctrl}} = -\Delta \dot{\boldsymbol{X}}_{\text{ctrl}}^T [P_2] \Delta \dot{\boldsymbol{X}}_{\text{ctrl}} \tag{24}$$

where $[P_2]$ is a 2×2 positive definite matrix. Substituting Eq. (23) into Eq. (24), yields:

$$[B_{\text{ctrl}}]\boldsymbol{\xi} = -k\Delta \boldsymbol{X}_{\text{ctrl}} - \boldsymbol{f}_{\text{ctrl}} - [P_2]\Delta \dot{\boldsymbol{X}}_{\text{ctrl}} \tag{25}$$

Note that $[B_{\text{ctrl}}]$ is a 2×3 matrix. As mentioned in the beginning of this section, there is a family of solutions of $\boldsymbol{\xi}$ that satisfy the control condition in Eq. (25). Let us begin with the minimum norm solution to Eq. (25):

$$\hat{\boldsymbol{\xi}} = [B_{\text{ctrl}}]^{\dagger}\big(- k\Delta \boldsymbol{X}_{\text{ctrl}} - \boldsymbol{f}_{\text{ctrl}} - [P_2]\Delta \boldsymbol{X}_{\text{ctrl}}\big) \tag{26}$$

where $[B_{\text{ctrl}}]^{\dagger} = [B_{\text{ctrl}}]^T([B_{\text{ctrl}}][B_{\text{ctrl}}]^T)^{-1}$ is the pseudo-inverse of the matrix $[B_{\text{ctrl}}]$. Note that $\hat{\boldsymbol{\xi}}$ in Eq. (26) is the minimum solution to Eq. (25) which minimizes the norm of the $\boldsymbol{\xi}$ vector. The general solution to Eq. (25) can be written as:

$$\boldsymbol{\xi} = \hat{\boldsymbol{\xi}} + \gamma \cdot \boldsymbol{b}_{\text{ctrl}} \tag{27}$$

where $\boldsymbol{b}_{\text{ctrl}}$ is a 3×1 base vector of the null space of the matrix $[B_{\text{ctrl}}]$. Because $[B_{\text{ctrl}}]$ is a 2×3 matrix, it always has a nonempty null space. The scalar parameter $\gamma \in \mathcal{R}$ can be any real number. The flexibility of the value of γ provides a single degree of freedom (DOF) that can be utilized to find an implementable (real spacecraft charge) control solution.

With the implementation problem having been narrowed down to finding a proper value of γ to make the solution $\boldsymbol{\xi}$ implementable, we rewrite the implementability criterion as:

$$\xi_1 \cdot \xi_2 \cdot \xi_3 \geq 0 \tag{28}$$

Substituting Eq. (27) into the criterion, yields:

$$g(\gamma) \triangleq \xi_1 \cdot \xi_2 \cdot \xi_3 = \big(\hat{\xi}_1 + \gamma b_{\text{ctrl}}(1)\big)\big(\hat{\xi}_2 + \gamma b_{\text{ctrl}}(2)\big)\big(\hat{\xi}_3 + \gamma b_{\text{ctrl}}(3)\big) \geq 0 \tag{29}$$

where $\hat{\xi}_i$ is given by the minimum norm solution in Eq. (26). The next step is to find a value of γ that satisfies the inequality $g(\gamma) \geq 0$. Note that $g(\gamma)$ is a cubic equation of γ. The two typical cases of the function $g(\gamma)$ are illustrated in Figure 3. In both cases, there are two continuous intervals of γ that make $g(\gamma) \geq 0$. This indicates that there always exists a family of solutions that make the 2-side control implementable with the same dynamical behavior.

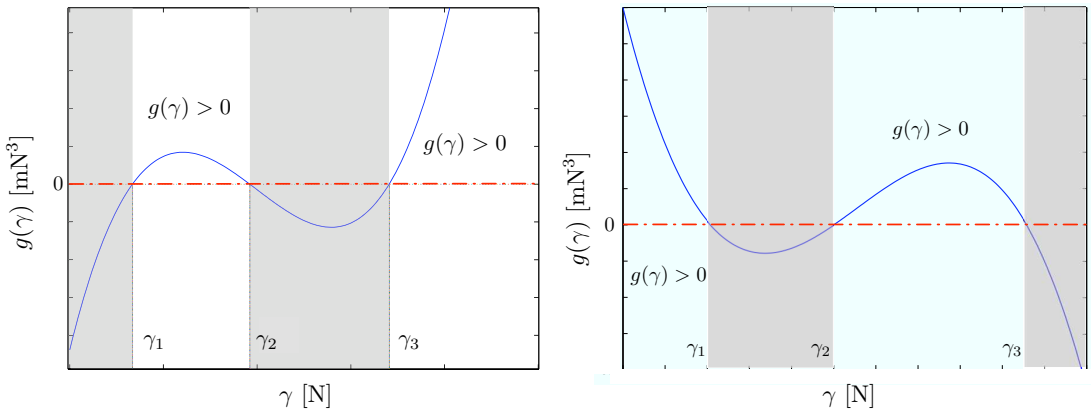

(a) $b_{\text{ctrl}}(1)b_{\text{ctrl}}(2)b_{\text{ctrl}}(3) > 0$. (b) $b_{\text{ctrl}}(1)b_{\text{ctrl}}(2)b_{\text{ctrl}}(3) < 0$.

Figure 3. Examples of $g(\gamma)$ function in two cases.

Because there is an infinite number of solutions that make the control implementable, a solution is chosen which minimizes the spacecraft charge magnitudes to simplify the technical implementation of this charge control solution. A charge cost function is defined:

$$J(\gamma) = \sum_{i=1}^{3} q_i^2 \tag{30}$$

Reference 18 develops an algorithm based on Newton's method to search the optimal solution of γ that minimizes the cost function $J(\gamma)$. The same algorithm is applied in this paper to determine the charge-optimal solution.

For a switched Lyapunov-based control, the stability needs to be reevaluated because the switching may introduce discontinuity to the Lyapunov candidate functions. The following property states that if the control is continuous then the switched control with the switch strategy given by Eq. (21) is stable.

Property 1 *The switched control strategy with the switch rule given by Eq.* (21) *is stable if* $\dot{V}_{ctrl} < 0$ *and the control is continuous, which indicates the switching happens when*

$$V_{ctrl} = max\{V_k | V_k = V_a, V_b, V_c \text{ and } V_k \neq V_{ctrl}\} \tag{31}$$

Proof Because the control is continuous, the Lyapunov function being controlled V_{ctrl} is continuous. Note that $\dot{V}_{\text{ctrl}} \leq 0$, the system is stable by Lyapunov stability theorem. □

In the ideal case with the control being continuous, the Lyapunov function being controlled is continuous and non-increasing. However, in praxis the control frequency is always limited resulting control cycles of finite duration. The discrete control time step makes the Lyapunov function being controlled discontinuous at the switch point. This discontinuity breaks down the stability proof based on continuous Lyapunov function. The next section utilizes a multiple Lyapunov function analysis tool to analyze the stability of the switched system and develops a stable switch strategy with present of the limited control time step.

MULTIPLE LYAPUNOV FUNCTIONS ANALYSIS

The last section designs a switching control strategy that always controls the "worst" two sides of the triangle, with the "worst" two sides defined by the corresponding Lyapunov function candidates. Stability is ensured if the switching can occur infinitely fast. The action of the switching may cause stability issues if the switching occurs over finite time steps. The tracking error of the uncontrolled triangle side can become the largest error during the finite control interval.

Multiple Lyapunov functions for switched systems[19] is a tool to analyze this type of systems with discretely switched control objectives. Before analyzing the switched system, let us define several concepts.

Definition A *switched system* is a simple case of a *hybrid system* that is of multi-modal, while the system switches in a way that there are finite switches in finite time.[19]

Definition *Control cycle period* is the time period while the control has to be constant without updating, it's limited by the hardware components such as sensors and actuators. The value of the control cycle period is constant.

Definition *Switch cycle period* is the time period during when the active Lyapunov function hasn't been switched. The value of the switch cycle period is not constant, the minimum possible value is equal to the control cycle period.

The switched control developed in the last section switches according to the three Lyapunov functions defined in Eq. (20). Now the switch frequency is constrained by the control cycle period. The maximum switch frequency is the inverse of the control cycle period. This satisfies the definition of the *switched system* that there are finite switches in finite time.

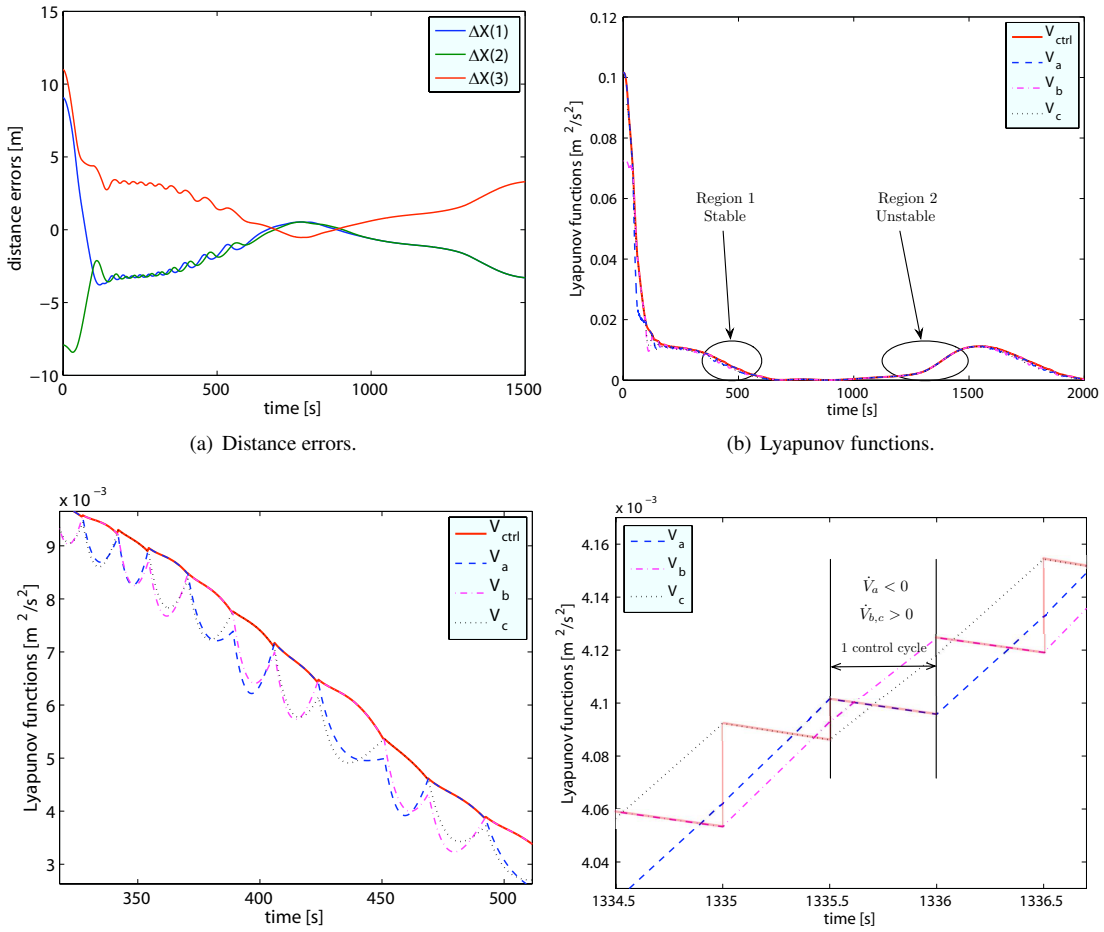

(a) Distance errors.

(b) Lyapunov functions.

(c) Stable switch.

(d) Unstable switch.

Figure 4. Simulation example of the unstable switch control strategy.

Stability Analysis

The stability of a *switched system* can not be characterized using only the Lyapunov stability theorem of a continuous system. Even when all the Lyapunov function rates of the activated models are negative semi-definite, the system can still be unstable due to the control objective switching.

Figure 4 shows a simulation example of the three-body Coulomb virtual structure control using the continuous control strategy developed in the previous section, but implemented with finite control cycles. Figure 4(a) shows the distance errors, Figures 4(b)–4(d) show the Lyapunov functions in different time ranges. The plots show that the system is stable during Region 1, but unstable during Region 2. Special tools should be engaged to explain and analyze this behavior.

Branicky's contribution in Reference 19 is a milestone in analyzing nonlinear hybrid system. He proves several theorems that justify the stability of different hybrid systems based on Lyapunov's stability theorem. This paper employs Theorem 2.3 from Reference 19 repeated here for clarity:

Theorem 1 *(Theorem 2.3 in Reference 19) Suppose we have candidate Lyapunov functions V_i, $i = 1, \cdots, N$ and vector fields $\dot{x} = f_i(x)$. Let $\mathcal{S}$ be the set of all switching sequences associated with the system.*

If for each $S \in \mathcal{S}$ we have that for all i, V_i is Lyapunov-like for f_i and $x_S(\cdot)$ over $S|i$, then the system is

stable in the sense of Lyapunov.

where "Lyapunov-like function" is defined as:

Definition (Reference 19) Given a strictly increasing sequence of times T in $\mathcal{R}$, we say that V is Lyapunov-like for function f and trajectory $x(\cdot)$ over T if:

- $\dot{V} \leq 0$ when it's activated
- V is monotonically nonincreasing on $\mathcal{E}(T)$

where $\mathcal{E}(T)$ denotes the even sequence of $T : t_0, t_2, t_4, \cdots$. $\square$

Theorem 1 explains the behavior in Figure 4. Figure 4(c) shows a snapshot at Region 1. It can be seen that at every other switching time, each Lyapunov function candidate is less than its value at the time point that is two switching cycles before. By Theorem 1, the Lyapunov function candidates (V_a, V_b, V_c) are Lyapunov-like and the system is stable in this region. Figure 4(d) is a snapshot during Region 2. In this case, the control switches at the maximum frequency and the switching cycle period is equal to the control cycle period. Even though during each control cycle the controlled Lyapunov function is decreasing, the un-controlled Lyapunov functions increase faster than the controlled Lyapunov function's decreasing rate. At every other switching time, each Lyapunov function candidate is greater than its value at the time that is two switching periods earlier. So the Lyapunov function candidates (V_a, V_b, V_c) is not Lyapunov-like during Region 2, and the system is unstable in this region.

The stability of the switched control strategy given by Eq. (21) and Eq. (27) is not guaranteed because the Lyapunov function candidates (V_a, V_b, V_c) are not guaranteed to be *Lyapunov-like*.

Switched Control Stability Requirements

Theorem 1 explains why the switched control strategy given by Eq. (21) and Eq. (27) can be unstable at times. This section improves the control strategy to make the Lyapunov function candidates V_a–V_c satisfy the *Lyapunov-like* conditions, such that the system is made stable even with discrete non-zero control cycles.

Assume that during one switching cycle V_β is the controlled Lyapunov function. The corresponding two sides being controlled are denoted as i^{th} and j^{th} sides, the uncontrolled side is the k^{th} side. Here "uncontrolled" doesn't mean the control won't affect the k^{th} side, but the k^{th} is not taken into consideration in developing the control algorithm. Note that when V_β is under control, the errors in the i^{th} and j^{th} sides are decreasing, but the trend of the error in the k^{th} side is undetermined.

Figure 4(d) shows an example that when V_a is decreasing, V_b and V_c are increasing at a very high rate. This means that the errors in the L_{12} and L_{13} sides are decreasing, but the error in the L_{23} side is increasing dramatically and destroys the stability of the system. To ensure stability of the system, the uncontrolled side's behavior can not be neglected.

Note that the control in Eq. (27) makes the errors in both of the two sides i^{th} and j^{th} decreasing. The error in the uncontrolled side needs to be investigated. Define three error functions in the same form as the Lyapunov function candidates:

$$V_1 = \frac{k}{2}\Delta X_1^2 + \frac{1}{2}\Delta \dot{X}_1^2, \quad V_2 = \frac{k}{2}\Delta X_2^2 + \frac{1}{2}\Delta \dot{X}_2^2, \quad V_3 = \frac{k}{2}\Delta X_3^2 + \frac{1}{2}\Delta \dot{X}_3^2 \tag{32}$$

Without loss of generality, rearrange the state vector in the form

$$\boldsymbol{X} = \begin{pmatrix} \boldsymbol{X}_{ctrl} \\ X_{uc} \end{pmatrix} \tag{33}$$

where $\boldsymbol{X}_{ctrl}$ is composed of two distance errors corresponding to the two controlled side, X_{uc} denote the distance error of the uncontrolled side. Correspondingly the EOM is rewritten to be:

$$\begin{pmatrix} \ddot{\boldsymbol{X}}_{ctrl} \\ \ddot{X}_{uc} \end{pmatrix} = \begin{bmatrix} [B_{ctrl}] \\ \boldsymbol{B}_{uc} \end{bmatrix} (\hat{\boldsymbol{\xi}} + \gamma \boldsymbol{b}_{ctrl}) + \begin{pmatrix} \boldsymbol{f}_{ctrl} \\ f_{uc} \end{pmatrix} \tag{34}$$

where $\boldsymbol{B}_{uc}$ is a 1×3 vector that is the line in the matrix $[B]$ corresponding to the uncontrolled side, f_{uc} is the component of the vector $\boldsymbol{f}$ corresponding to the uncontrolled side. Substituting $\hat{\boldsymbol{\xi}}$ in Eq. (26) into Eq. (34) and carrying out the algebra, yields:

$$\begin{pmatrix} \ddot{\boldsymbol{X}}_{ctrl} \\ \ddot{X}_{uc} \end{pmatrix} = \begin{pmatrix} -k\Delta \boldsymbol{X}_{ctrl} - [P_2]\Delta \dot{\boldsymbol{X}}_{ctrl} \\ \boldsymbol{B}_{uc}[B_{ctrl}]^{\dagger}\big(-k\Delta \boldsymbol{X}_{ctrl} - [P_2]\Delta \dot{\boldsymbol{X}}_{ctrl} - \boldsymbol{f}_{ctrl}\big) + \gamma \boldsymbol{B}_{uc}\boldsymbol{b}_{ctrl} + f_{uc} \end{pmatrix} \tag{35}$$

Taking a time derivative of the error function of the uncontrolled side V_{uc} and substituting $\ddot{X}_{uc}$, yield:

$$\begin{aligned} \dot{V}_{uc} =& k\Delta \dot{X}_{uc}(\Delta X_{uc} + \Delta \ddot{X}_{uc}) \\ =& k\Delta \dot{X}_{uc}\Big(\Delta X_{uc} + \boldsymbol{B}_{uc}[B_{ctrl}]^{\dagger}\big(-k\Delta \boldsymbol{X}_{ctrl} - [P_2]\Delta \dot{\boldsymbol{X}}_{ctrl} - \boldsymbol{f}_{ctrl}\big) + \gamma \boldsymbol{B}_{uc}\boldsymbol{b}_{ctrl} + f_{uc}\Big) \end{aligned} \tag{36}$$

Eq. (36) shows that the sign of the uncontrolled side's error is undetermined. Even though there are two parameters $[P_2]$ and γ that can be adjusted, this flexibility doesn't guarantee there exists a solution to make $\dot{V}_{uc}$ negative because in some cases controlling three sides is impossible.

To find a way to solve this problem, it is beneficial to take a closer look at the unstable situation shown in Figure 4(d). Note that the three Lyapunov function candidates are actually the combinations of the error functions:

$$V_a = V_1 + V_3, \quad V_b = V_1 + V_2, \quad V_c = V_2 + V_3 \tag{37}$$

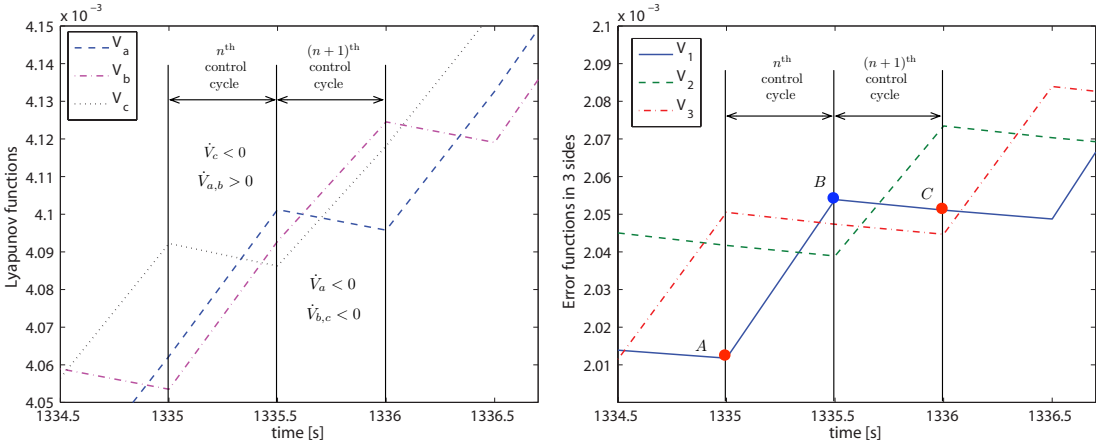

(a) Lyapunov function candidates.

(b) Error functions.

Figure 5. Unstable switch analysis.

Figure 5 shows the details of the Lyapunov function candidates and the error functions during several unstable switches. In Figure 5(a), during the n^{th} switch cycle, $\dot{V}_c < 0$ while $\dot{V}_a$ and $\dot{V}_b$ are positive. $\dot{V}_c < 0$ indicates $\dot{V}_2 < 0$ and $\dot{V}_3 < 0$. This is verified by Figure 5(b). So $V_{a,b} > 0$ is due to the excessive increasing of V_1, as shown in Figure 5(b). At the beginning of the next control cycle, $(n+1)^{\text{th}}$ control cycle, it is identified that V_a is the largest Lypunov function candidate. According to the switch strategy in Eq. (21), the controller

switches to control V_a which indicates $V_{1,3} < 0$ as shown in Figure 5(b). Focusing on V_1 in Figure 5(b), one can see that during the $(n+1)^{\text{th}}$ control cycle, V_1 is controlled such that $\dot{V}_1 < 0$. But the rate of decreasing of V_1 is smaller than its increasing rate during the n^{th} control cycle. This results in that at the next switch time (at the point C in Figure 5(b)), V_1 hasn't decreased to the same level as the value at the beginning of the n^{th} control cycle (at the point A). That is $V_1^{(C)} > V_1^{(A)}$. According to Branicky's theorem in Theorem 1, V_1 is not *Lyapaunov-like* and the stability is not guaranteed.

By the above analysis, it can be concluded that the instability comes from two sources:

1. The decreasing rate of the error function of the new controlled side is not big enough to compensate for its increased amount during the last control cycle.

2. The increasing rate of the error function of the new uncontrolled side is too big.

Upon entering a new control objective switch, both the new uncontrolled and the new controlled sides' error functions need to be taken care of to ensure the Lyapunov function candidates to be *Lyapunov-like*. Corresponding to Figure 5(b), the magnitude of the slope of V_1 during the $(n+1)^{\text{th}}$ control cycle should be greater than the slope during the n^{th} control cycle. The increasing rate of V_2 during the $(m+1)^{\text{th}}$ control cycle should be less than its decreasing rate during the n^{th} control cycle. Figure 6 illustrates this idea. In this way, $V_1^{(C)} < V_1^{(A)}$ and $V_2^{(C)} < V_2^{(A)}$. V_3 is always being controlled during the two control cycles so it's automatically satisfied that $V_3^{(c)} < V_3^{(A)}$. Thus all of the Lyapunov function candidates are *Lyapunov-like* during the two control cycles.

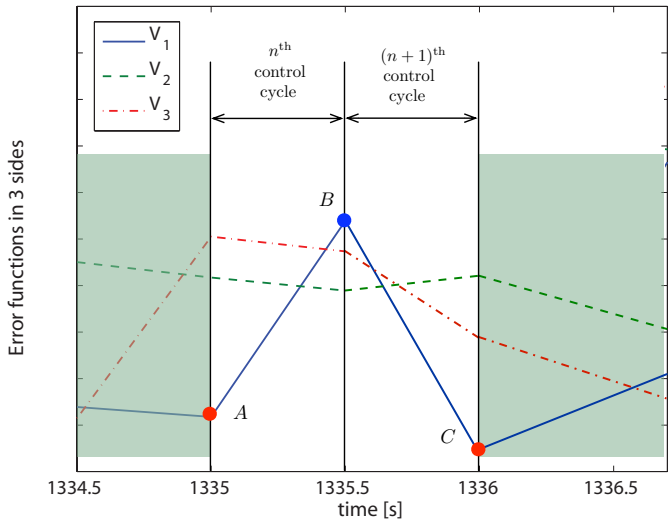

Figure 6. Hand-Drawn Illustration of the new switch strategy effect.

To take care of the new controlled side, which indicates this side was uncontrolled in the last control cycle, the first step is to determine the requirement to remain Lyapunov-like for this side. Let V_m denote the new controlled side's error function. The requirement for this side to be *Lyapunov-like* is that the change of the corresponding error function in the new switch cycle $\Delta V_m^{(n+1)}$ should be less than its change in the previous switch cycle $\Delta V_m^{(n)}$. This can be expressed mathematically in the way:

$$\int_{(n+1)} \dot{V}_m^{(n+1)} dt < -\Delta V_m^{(n)} \tag{38}$$

where $\int_{(n+1)}$ means the integration across the $(n+1)^{\text{th}}$ switch cycle. Because the control cycle period is very small, the inequality in Eq. (38) is approximated by

$$\dot{V}_m^{(n+1)}\Delta t < -\Delta V_m^{(n)} \tag{39}$$

where Δt is the control cycle period which is constant. This requires the error function rate $\dot{V}_m^{(n+1)}$ should be less than a certain value:

$$\dot{V}_m^{(n+1)} < -\Delta V_m^{(n)}/\Delta t \tag{40}$$

Because the subscript m denotes the new controlled side, $\dot{V}_m^{(n+1)}$ is determined to be negative. If $\Delta V_m^{(n)}$ is negative which means V_m decreases in the n^{th} control cycle, then the requirement in Eq. (40) is automatically satisfied. Otherwise, a strategy that makes the inequality in Eq. (42) always satisfied is expected. Taking a time derivative of V_m then substituting the EOM of X_m in Eq. (34) yields:

$$\dot{V}_m = \Delta\dot{X}_m\Big(k\Delta X_m + \boldsymbol{B}_m[B_{ctrl}]^{\dagger}(-k\Delta\boldsymbol{X}_{ctrl} - [P_2]\Delta\dot{\boldsymbol{X}}_{ctrl} - \boldsymbol{f}_{ctrl}) + \boldsymbol{f}_m\Big) \tag{41}$$

In this expression of $\dot{V}_m$ only the control coefficients k and $[P_2]$ are not dependent on the states and can be utilized to adjust the value of $\dot{V}_m$. This paper choose to change the matrix $[P_2]$ to make the error functions to be *Lyapunov-like*. Substituting Eq. (41) into the inequality in Eq. (42), yields:

$$\begin{aligned}\Delta\dot{X}_m\boldsymbol{B}_m[B_{ctrl}]^{\dagger}[P_2]\Delta\dot{\boldsymbol{X}}_{ctrl} >& \Delta\dot{X}_m\Big(k\Delta X_m + f_m \\ &+ \boldsymbol{B}_m[B_{ctrl}]^{\dagger}(-k\Delta\boldsymbol{X}_{ctrl} - \boldsymbol{f}_{ctrl})\Big) + \frac{\Delta V_m^{(n)}}{\Delta t}\end{aligned} \tag{42}$$

The inequality in Eq. (42) is the requirement for the matrix $[P_2]$ that ensures the error function of the new controlled side is *Lyapunov-like*. The requirement for the new uncontrolled side is similar:

$$\begin{aligned}\Delta\dot{X}_{uc}\boldsymbol{B}_{uc}[B_{ctrl}]^{\dagger}[P_2]\Delta\dot{\boldsymbol{X}}_{ctrl} >& \Delta\dot{X}_{uc}\Big(k\Delta X_{uc} + f_{uc} \\ &+ \boldsymbol{B}_{uc}[B_{ctrl}]^{\dagger}(-k\Delta\boldsymbol{X}_{ctrl} - \boldsymbol{f}_{ctrl})\Big) + \frac{\Delta V_{uc}^{(n)}}{\Delta t}\end{aligned} \tag{43}$$

The inequalities in Eqs. (42), (43) are two conditions that guarantees the error functions to be *Lyapunov-like*. Note that the matrix $[P_2]$ should be positive definite, so there are three requirements for $[P_2]$ that ensures a globally stable switched control.

Stable Switched Strategy

The previous section determined three requirements that ensured a stable switched control. This section develops a new switched control strategy that implements the stability requirements found in Eqs. (42) and (43). Above all, the existence of solutions that satisfy the stability requirements needs to be investigated. Let us begin with introducing an asymmetric positive definite matrix.

Property 2 *A 2×2 matrix $[P]$ in the form*

$$[P] = \begin{bmatrix} p_{11} & p_{12} \\ -p_{12} & p_{22} \end{bmatrix} \tag{44}$$

is a positive definite matrix if and only if:

$$p_{11} > 0, \quad p_{22} > 0. \tag{45}$$

Proof The symmetric part of the matrix $[P]$ is:

$$[P_s] = \frac{1}{2}[P] + \frac{1}{2}[P]^T = \begin{bmatrix} p_{11} & 0 \\ 0 & p_{22} \end{bmatrix} \tag{46}$$

It is evident that the symmetric matrix $[P_s]$ is positive definite if and only if $p_{11} > 0$ and $p_{22} > 0$. A necessary and sufficient condition for a real matrix to be positive definite is that its symmetric part is positive definite. Thus the matrix $[P]$ is positive definite if and only if $p_{11} > 0$ and $p_{22} > 0$. $\square$

This form of a positive definite matrix is more general than symmetric positive definite matrices. This provides more flexibilities in solving the inequalities in Eqs. (42) and (43). Note that the inequalities in Eqs. (42) and (43) can be written in the general form:

$$\boldsymbol{a}^T[P_2]\boldsymbol{b} > c \tag{47}$$

where $\boldsymbol{a}$ and $\boldsymbol{b}$ are two 2-dimensional vectors, c is a real number that equals the right hand side (RHS) of the inequalities. The following theorem studies the existence of the solutions to this inequality.

Theorem 2 *Assume a positive definite matrix in the form:*

$$[P] = \begin{bmatrix} p_{11} & p_{12} \\ -p_{12} & p_{22} \end{bmatrix} \tag{48}$$

where p_{11} and p_{22} are positive. Define two arrays: $\boldsymbol{a} = [a_1,\ a_2]^T$ and $\boldsymbol{b} = [b_1,\ b_2]^T$. If the following two inequalities and equation do not happen at the same time:

$$a_1 b_1 < 0, \tag{49a}$$
$$a_2 b_2 < 0, \tag{49b}$$
$$a_2 b_1 = a_1 b_2 \tag{49c}$$

then for any $c \in \mathbb{R}$, there always exists a solution of the matrix $[P]$ that satisfies the inequality:

$$\boldsymbol{a}^T[P]\boldsymbol{b} > c. \tag{50}$$

Proof Let us prove that the solution of $[P]$ exists under the following two cases:

1. $a_2 b_1 \neq a_1 b_2$,
2. $a_2 b_1 = a_1 b_2$ and $a_1 b_1 > 0$ and/or $a_2 b_2 > 0$.

Carrying out the algebra in the inequality in Eq. (48), yields:

$$a_1 b_1 p_{11} + (a_1 b_2 - a_2 b_1) p_{12} + a_2 b_2 p_{22} > c \tag{51}$$

Note that the requirements for p_{ij} are $p_{11} > 0$ and $p_{22} > 0$, the third element p_{12} can be any real number. Next the existence of the positive definite matrix $[P]$ is proven under the enumerated two cases.

Case 1: $a_2 b_1 \neq a_1 b_2$. When $a_2 b_1 \neq a_1 b_2$, the element p_{12} can be used to adjust the value of the left hand side (LHS) of the inequality in Eq. (51). If $a_1 b_2 > a_2 b_1$, then any real value of p_{12} that satisfies:

$$p_{12} > \frac{c - a_1 b_1 p_{11} - a_2 b_2 p_{22}}{a_1 b_2 - a_2 b_1} \tag{52}$$

is a solution to the inequality in Eq. (48) while preserving the positive definiteness of the matrix $[P]$. Alternatively if $a_1 b_2 < a_2 b_1$, then any real value of p_{12} that satisfies:

$$p_{12} < \frac{c - a_1 b_1 p_{11} - a_2 b_2 p_{22}}{a_1 b_2 - a_2 b_1} \tag{53}$$

is a solution to the inequality in Eq. (48).

Case 2: $a_2b_1 = a_1b_2$ *and* $a_1b_1 > 0$ *and/or* $a_2b_2 > 0$. When $a_2b_1 = a_1b_2$, the inequality in Eq. (51) simplifies to

$$a_1b_1p_{11} + a_2b_2p_{22} > c \tag{54}$$

Because either $a_1b_1 > 0$ or $a_2b_2 > 0$, without loss of generality it's supposed $a_1b_1 > 0$. Solving for p_{11} from the inequality in Eq. (54), yields:

$$p_{11} > \frac{1}{a_1b_1}(c - a_2b_2p_{22}) \tag{55}$$

The inequality in Eq. (55) does not conflict with the requirement that $p_{11} > 0$. Thus any value of p_{11} that satisfies:

$$p_{11} > \max\left\{\frac{1}{a_1b_1}(c - a_2b_2p_{22}),\ 0\right\} \tag{56}$$

is a solution to the inequality in Eq. (48). □

Theorem 2 proves the existence of solutions to the inequalities in Eqs. (42) and (43) unless the condition in Eq. (49) occurs. Note that the two inequalities and one equation in Eq. (49) are rarely to happen at the same time. Moreover, $a_1b_2 = a_2b_1$ is a transient state. Generally this situation is neglectable.

Now all steps are in place to lay out the new stable switched charge control strategy. Note that the old switched control strategy works well most of the time, the temporary loss of stability happens due to the discrete control time steps. The first switch strategy given by Eq. (21) is still valid unless the *Lyapunov-like* condition being violated.

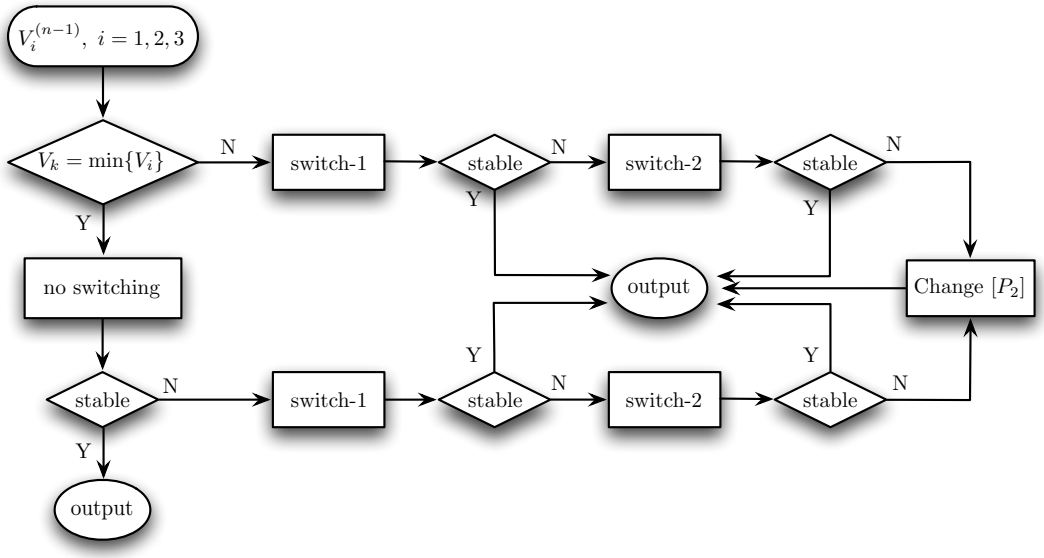

Figure 7. Stable switch strategy flowchart.

Beginning a new control cycle, there are three possible combinations of the controlled sides. One of them corresponds to no switching case, the other two correspond to two switched control cases. For the notational convenience, denote the three possibilities as "no switching", "switch-1" and "switch-2". When an unstable

switching, which means the switching doesn't satisfy the requirements in Eqs. (42) and (43), is detected, it is easier to change the new controlled side than to change the value of the matrix $[P_2]$. Based on this rule, a new switch strategy is developed and shown in Figure 7.

Figure 7 illustrates the strategy of switching. The details of calculating the value of the matrix $[P_2]$ is not illustrated. Upon changing the value of $[P_2]$, it's better to start with simpler diagonal form. If the diagonal form of $[P_2]$ matrix cannot provide a stable switched control, then the more complex asymmetric matrix form as shown in Eq. (48) is sought.

NUMERICAL SIMULATIONS

This section presents numerical simulations to show the effectiveness and performance of the stable switched 3-craft charge control. The desired shape here is triangular configuration. For notational convenience, the old controller with the switching strategy given by Eq. (21) is called Controller-1, the new stable controller with the switching strategy given by Figure 7 is called Controller-2.

Both Controller-1 and Controller-2 are used to control the 3-craft Coulomb virtual structure. Under the same initial conditions the performances of the two controllers can be compared. The response of the system is different in different situations. When the initial errors and separation distances are large, the control charges levels are large. The following two simulation cases illustrate the behavior of the system under two controllers. In all of the simulations the masses of the three spacecraft are the same:

$$m_1 = m_2 = m_3 = 50 \text{ kg} \tag{57}$$

Big Control Effort Case

The initial positions and velocities of the three spacecraft are

$$\begin{cases} \boldsymbol{r}_1 = [9, -2, 0]^T \text{ m} \\ \boldsymbol{r}_2 = [0, -4, 0]^T \text{ m} \\ \boldsymbol{r}_3 = [-2, -2, 0]^T \text{ m} \end{cases}, \quad \begin{cases} \dot{\boldsymbol{r}}_1 = [0, 0.01, 0]^T \text{ m/s} \\ \dot{\boldsymbol{r}}_2 = [0, 0, 0]^T \text{ m/s} \\ \dot{\boldsymbol{r}}_3 = [0, -0.01, 0]^T \text{ m/s} \end{cases} \tag{58}$$

The expected triangular shape of the virtual structure is defined by the separation distances:

$$\boldsymbol{X}^* = [6, 7, 5]^T \text{ m} \tag{59}$$

The proportional feedback coefficients are:

$$k = 0.0003 \text{ s}^{-2} \tag{60}$$

The nominal value of the matrix $[P_2]$ is

$$[P_2^*] = \begin{bmatrix} 0.02 & 0 \\ 0 & 0.02 \end{bmatrix} \text{ s}^{-1} \tag{61}$$

Note that the value of the $[P_2]$ matrix is varying using Controller-2.

Figure 8 shows the responses of the system under the two different control strategy. Comparing the separation distance errors in Figures 8(a) and 8(b), it is evident that the stable switched control strategy performs better than the unstable switched control. Using this set of initial states and controller parameters, the old controller assuming continuos switching capabilities cannot stabilize the distance errors to zero, while the stable switched control strategy with finite control cycles stabilizes the errors near zero. Because the rotating triangular configuration is not an equilibrium solutions, the errors cannot converge perfectly to zero. The smaller the control cycles are, the smaller the final state errors will become.

The error functions' histories in Figure 8(c) explains the behavior of the continuous-switching controller. During the time around 700–1000s, the controller switches at the highest frequency and the error functions

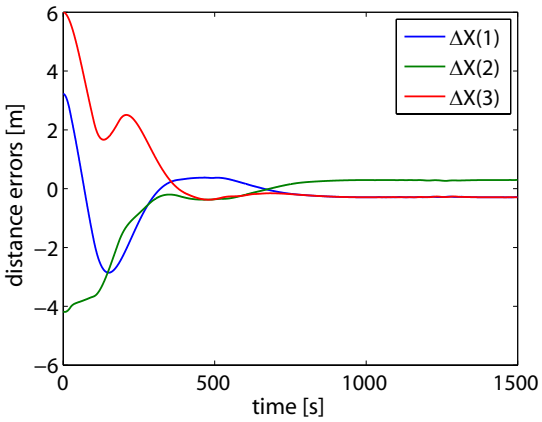

(a) Separation distance errors, Controller-1.

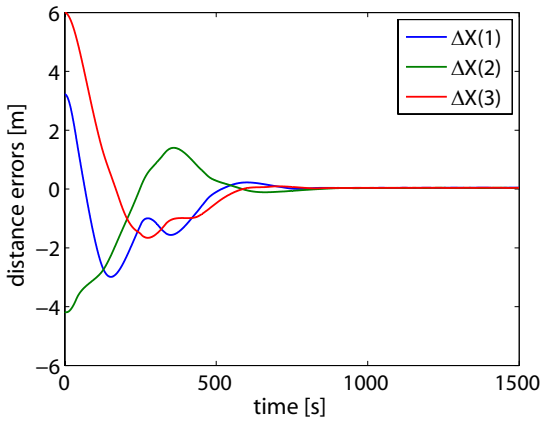

(b) Separation distance errors, Controller-2.

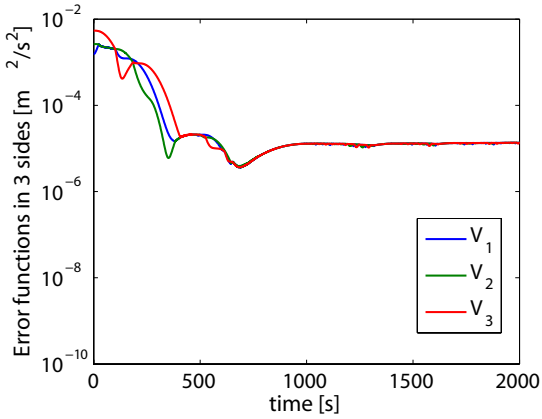

(c) Error functions, Controller-1.

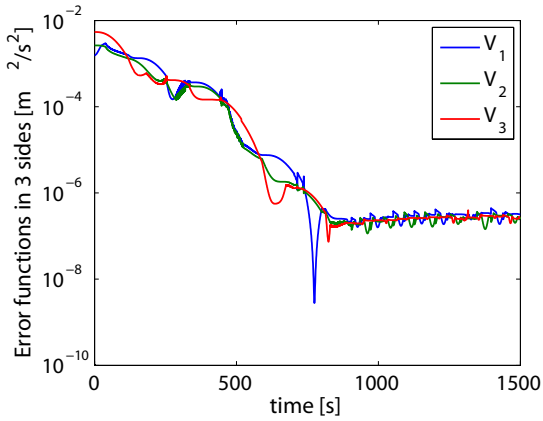

(d) Error functions, Controller-2.

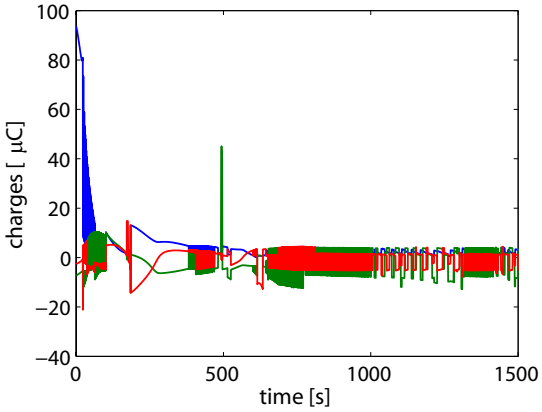

(e) Charges, Controller-1.

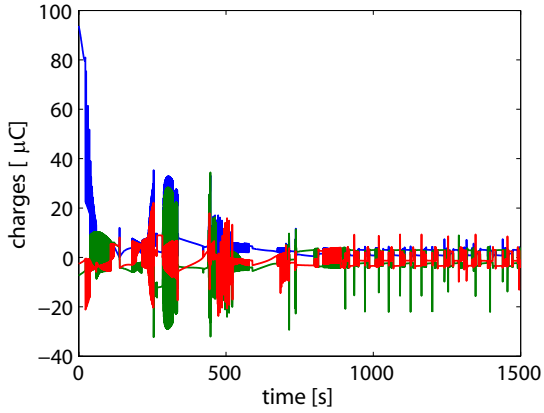

(f) Charges, Controller-2.

Figure 8. Big control effort simulations.

don't satisfy the *Lyapunov-like* conditions. The details are similar to Figure 5(b). Thus this is an unstable part of the response. Figure 8(d) shows that under the control of the stable switched control strategy, the error functions drop to very low level (10^{-7}m^2/s^2) within 1000s, but won't really decrease to zero. This means the system is stable, but not asymptotically stable as explained above.

Figures 8(e) and 8(f) show the charge histories of the two simulations. It can be seen that under the control of the stable switched controller, the charge histories have more spikes than that of the unstable switched control. This is due to the variation of the matrix $[P_2]$ in the stable switched control. Despite the spikes in the charge histories, it can be seen that after the distance errors settle down (after 800s as shown in Figure 8(b)), the control charge level that holds the spinning triangle is around 5μC. But at the beginning the charge level goes up to 90μC which is not practically implementable. The practically implementable charge level is within 10μC. This simulation case is aggressive. The intention is to show the different behaviors under different situations.

Small Control Effort Case

In this simulation, the initial errors and the separation distances are small thus the controllers require small charge levels. The initial conditions are set as

$$\begin{cases} \boldsymbol{r}_1 = [2,\ 0,\ 0]\ \text{m} \\ \boldsymbol{r}_2 = [0,\ -4,\ 0]\ \text{m} \\ \boldsymbol{r}_3 = [-2,\ -2,\ 0]\ \text{m} \end{cases} \quad \begin{cases} \dot{\boldsymbol{r}}_1 = [0,\ 0.002,\ 0]\ \text{m/s} \\ \dot{\boldsymbol{r}}_2 = [0,\ 0,\ 0]\ \text{m/s} \\ \dot{\boldsymbol{r}}_3 = [0,\ -0.002,\ 0]\ \text{m/s} \end{cases} \tag{62}$$

The expected separation distances are given by:

$$\boldsymbol{X}^* = [4,\ ,4,\ 4]^T\ \text{m} \tag{63}$$

The controller coefficients are

$$k = 0.0003\ \text{s}^{-2}, \quad [P_2^*] = \text{diag}(0.005,\ 0.005)\ \text{s}^{-1} \tag{64}$$

Figure 9 shows the simulation results under the two controllers. Figures 9(a), 9(c) and 9(e) show the results of the simulation using Controller-1. The distance error history in Figure 9(a) shows that at the beginning 2000s, the errors are staying at high level. The error functions shown in Figure 9(e) verify that during [0,2000]s, there are several temporary unstable regions where both of the three error functions are increasing. After 2000s, the distance errors are decreasing significantly.

Figures 9(b), 9(d) and 9(f) show the results of the simulation using Controller-2. Figure 9(b) shows that the distance errors decrease and stabilize to zero in much shorter time than using Controller-1. Comparing the charge histories in Figures 9(c) and 9(d), it can be seen that there are more spikes when Controller-2 is being used. Figure 9(b) also shows that the distance errors do not converge to zero. This is because the new switched control Controller-2 is stable, but not converging.

It's not always the case that Controller-2 performs better than Controller-1. Under different initial conditions and controller coefficients Controller-1 may perform better than Controller-2. There is one difference between the two simulation cases. When using Controller-1 in the large control effort case in the illustrated simulation results, the distance errors settles down to a certain level and stack there. But in the small control effort case, the distance errors keep changing, do not stay at a certain level.

CONCLUSION

This paper studies a three-spacecraft Coulomb formation triangular shape control problem. Assuming continuous switching capability, a 2-side switched control strategy is developed to always control the worst two sides instead of controlling both of the three sides. Here an implementable control solution is always guaranteed. However, the discrete control time steps may cause temporary instability of the shape control. A stable switched control strategy is developed based on the multiple Lyapunov functions analysis. This new

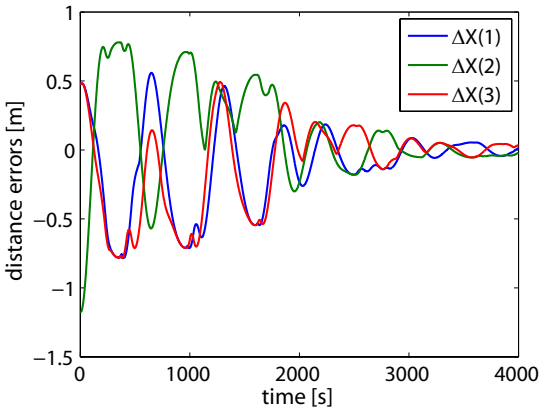

(a) Separation distance errors, Controller-1.

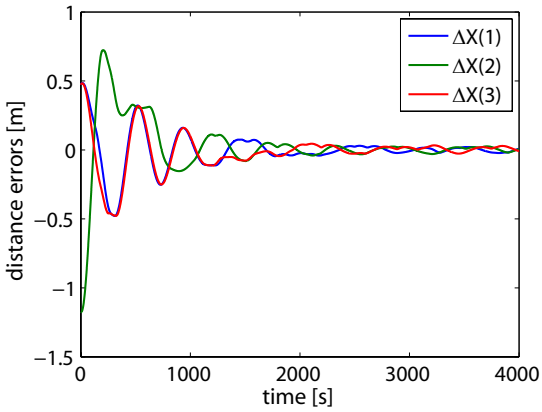

(b) Separation distance errors, Controller-2.

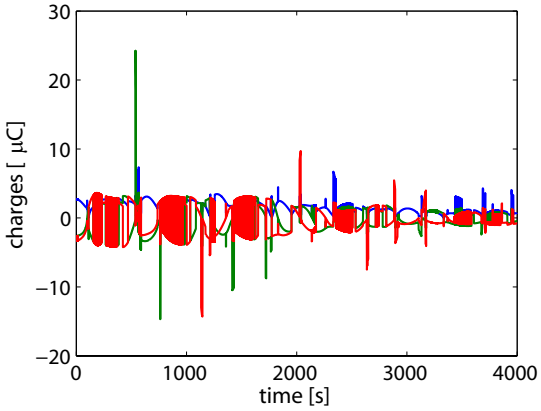

(c) Charges, Controller-1.

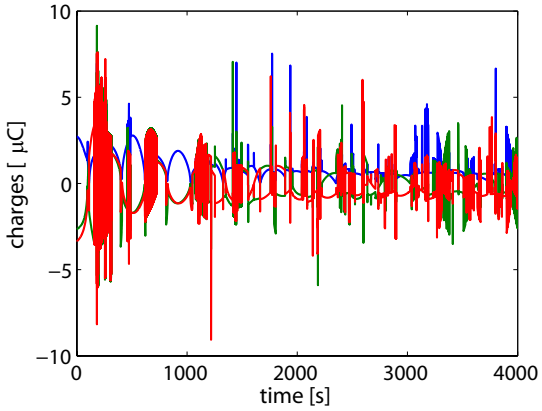

(d) Charges, Controller-2.

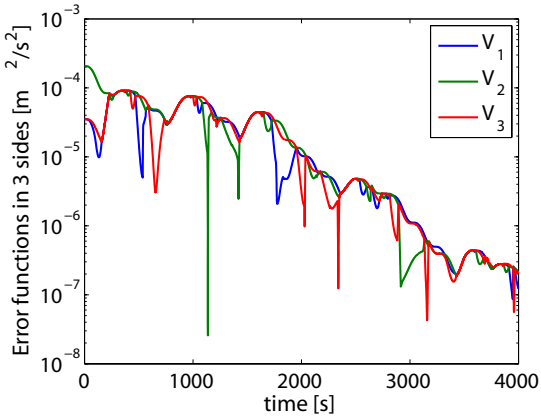

(e) Error functions, Controller-1.

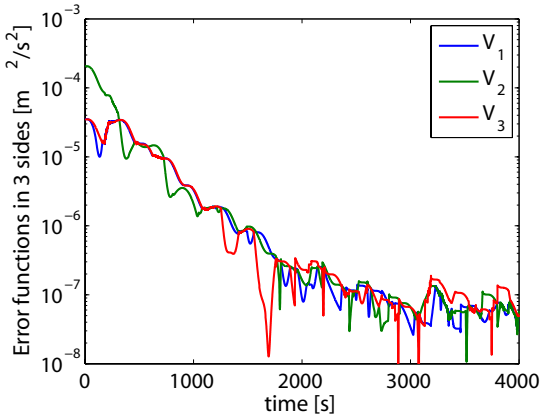

(f) Error functions, Controller-2.

Figure 9. Small control effort simulations.

switch strategy ensures all of the error functions to be *Lyapunov-like* thus stability is guaranteed. Numerical simulations demonstrate the improvement of the stable switched control. The new switched control also induces spikes in the control charges because the new control changes the value of the distance rate feedback gain matrix to ensure stability. The method of employing Lyapunov-like control functions is a promising approach to investigate the relative control of charged spacecraft with more than 3 vehicles. The new switched control strategy is successful in stabilizing a non-equilibrium triangular shape. Future work will investigate how this control can be utilized to control 3-craft collinear equilibrium shapes.

REFERENCES

[1] W. Ren and R. W. Beard, "Virtual Structure Based Spacecraft Formation Control With Formation Feedback," *AIAA Guidance, Navigation and Control Conference and Exhibit*, Monterey, California, 5-8 Aug 2002.

[2] L. B. King, G. G. Parker, S. Deshmukh, and J.-H. Chong, "Spacecraft Formation-Flying using Inter-Vehicle Coulomb Forces," tech. rep., NASA/NIAC, January 2002. `http://www.niac.usra.edu`.

[3] J. Berryman and H. Schaub, "Static Equilibrium Configurations in GEO Coulomb Spacecraft Formations," *15th AAS/AIAA Space Flight Mechanics Meeting*, Jan. 23–27 2005.

[4] J. Berryman and H. Schaub, "Analytical Charge Analysis for 2- and 3-Craft Coulomb Formations," *AAS/AIAA Astrodynamics Specialists Conference*, Lake Tahoe, CA, Aug. 7–11, 2005 2005. Paper No. 05-278.

[5] H. Schaub, C. Hall, and J. Berryman, "Necessary Conditions for Circularly-Restricted Static Coulomb Formations," *AAS Malcolm D. Shuster Astronautics Symposium*, Buffalo, NY, June. 12–15 2005. Paper No. AAS 05–472.

[6] H. Vasavada and H. Schaub, "Analytic Solutions for Equal Mass 4-Craft Static Coulomb Formation," *AAS/AIAA Astrodynamics Specialists Conference*, Mackinac Island, MI, Aug. 19–23 2007. Paper AAS 07–268.

[7] A. Natarajan and H. Schaub, "Linear Dynamics and Stability Analysis of a Coulomb Tether Formation," *AIAA Journal of Guidance, Control, and Dynamics*, Vol. 29, July–Aug. 2006, pp. 831–839.

[8] A. Natarajan and H. Schaub, "Hybrid Conrol of Orbit Normal and Along-Track 2-Craft Coulomb Tethers," *AAS Space Flight Mechanics Meeting*, Sedona, AZ, Jan. 28–Feb. 1 2007. Paper AAS 07–193.

[9] A. Natarajan, H. Schaub, and G. G. Parker, "Reconfiguration of a 2-Craft Coulomb Tether," *AAS Space Flight Mechanics Meeting*, Tampa, FL, Jan. 22–26 2006. Paper No. AAS-06-229.

[10] A. Natarajan and H. Schaub, "Orbit-Nadir Aligned Coulomb Tether Reconfiguration Analysis," *AAS/AIAA Spaceflight Mechanics Meeting*, Galveston, TX, Jan. 27–31 2008. Paper AAS 08–149.

[11] V. Lappas, C. Saaj, D. Richie, M. Peck, B. Streeman, and H. Schaub, "Spacecraft Formation Flying and Reconfiguration with Electrostatic Forces," *AAS/AIAA Space Flight Mechanics Meeting*, Sedona, AZ, Jan. 28–Feb. 1 2007. Paper AAS 07–113.

[12] S. Wang and H. Schaub, "Spacecraft Collision Avoidance using Coulomb Forces with Separation Distance And Rate Feedback," *AIAA Journal of Guidance, Control and Dynamics*, Vol. 33, May–June 2008, pp. 740–750.

[13] S. Wang and H. Schaub, "Open-Loop Electrostatic Spacecraft Collision Avoidance Using Patched Conics Analysis," *AAS/AIAA Spaceflight Mechanics Meeting*, Galveston, TX, Jan. 27–31 2008. Paper AAS 08–207.

[14] S. Wang and H. Schaub, "Electrostatic Spacecraft Collision Avoidance Using Piece-Wise Constant Charges," *AAS/AIAA Space Flight Mechanics Meeting*, Savannah, GA, February 8–12 2009. Paper AAS 09-184.

[15] I. I. Hussein and H. Schaub, "Invariant Shape Solutions of the Spinning Three Craft Coulomb Tether Problem," *AAS Space Flight Mechanics Meeting*, Tampa, Florida, January 22–26 2006. Paper No. AAS 06-228.

[16] H. Schaub and I. I. Hussein, "Stability and Reconfiguration Analysis of a Circulary Spinning 2-Craft Coulomb Tether," *IEEE Aerospace Conference*, Big Sky, MT, March 3–10 2007.

[17] I. I. Hussein and H. Schaub, "Stability and Control of Relative Equilibria for the Three-Spacecraft Coulomb Tether Problem," *AAS/AIAA Astrodynamics Specialists Conference*, Mackinac Island, MI, Aug. 19–23 2007. Paper AAS 07–269.

[18] S. Wang and H. Schaub, "1-D Constrained Coulomb Structure Stabilization With Charge Saturation," *AAS/AIAA Astrodynamics Specialists Conference*, Mackinac Island, MI, Aug. 19–23 2007. Paper AAS 07–267.

[19] M. S. Branicky, "Multiple Lyapunov Functions and Other Analysis Tools for Switched and Hybrid Systems," *IEEE Transactions on Automatic Control*, Vol. 43, April 1998, pp. 475–482.